Poly(2-isopropyl-2-oxazoline)-*b*-Poly(lactide) (PiPOx-*b*-PLA) nanoparticles in water: interblock van der Waals attraction opposes amphiphilic phase separation

*Fabian Pooch,[1] Marjolein Sliepen,[1] Kenneth D. Knudsen,[2] Bo Nyström,[3] Heikki Tenhu[1], Françoise M. Winnik,[1,4]**

1 Department of Chemistry, University of Helsinki, P.O. Box 55, Helsinki 00014, Finland

2 Department of Physics, Institute for Energy Technology, P.O. Box 40, N-2027 Kjeller, Norway

3 Department of Chemistry, University of Oslo, P.O. Box 1033, Blindern, N-0315 Oslo, Norway

4 International Center for Materials Nanoarchitectonics, National Institute for Materials Science, 1-1 Namiki, Tsukuba 305-0044, Japan

* To whom correspondence should be addressed (francoise.winnik@helsinki.fi)

Author information:

Fabian Pooch: 0000-0003-1925-1072
Marjolein Sliepen: 0000-0001-7148-9796
Kenneth D. Knudsen: 0000-0003-3091-2134
Bo Nyström: 0000-0002-6903-4423
Heikki Tenhu: 0000-0001-5957-4541
Françoise M. Winnik: 0000-0001-5844-6687

Abstract:

Poly(2-isopropyl-2-oxazoline)-*b*-Poly(lactide) (PiPOx-*b*-PLA) diblock copolymers comprise two miscible blocks: the hydrophilic and thermosensitive PiPOx and the hydrophobic PLA, a biocompatible and biodegradable polyester. They self-assemble in water, forming stable dispersions of nanoparticles with hydrodynamic radii (R_h) ranging from ~ 18 nm to 60 nm, depending on their molar mass, the relative size of the two blocks, and the configuration of the lactide unit. Evidence from ^{1}H nuclear magnetic resonance spectroscopy, light scattering, small angle neutron scattering, and cryo-transmission electron microscopy indicate that the nanoparticles do not adopt the typical core-shell morphology. Aqueous nanoparticle dispersions heated from 20 °C to 80 °C were monitored by turbidimetry and microcalorimetry. Nanoparticles of copolymers containing a poly(DL-lactide) block coagulated irreversibly upon heating to 50 °C, forming particles of various shapes (R_h ~ 200 – 500 nm). Dispersions of PiPOx-*b*-poly(L-lactide) coagulated to a lesser extend or remained stable upon heating. From the entire experimental evidence, we conclude that PiPOx-*b*-PLA nanoparticles consist of a core of PLA/PiPOx chains associated via dipole-dipole interactions of the PLA and PiPOx carbonyl groups. The core is surrounded by tethered PiPOx loops and tails responsible for the colloidal stability of the nanoparticles in water. While the core of all nanoparticles studied contains associated PiPOx and PLA blocks, fine details of the nanoparticles morphology vary predictably with the size and composition of the copolymers, yielding particles of distinctive thermo-sensitivity in aqueous dispersions.

Introduction:

In selective solvents, diblock copolymers (BCPs) tend to self-assemble into core-corona structures above their critical micelle concentration (cmc),[1] as it is the case for surfactants, their low molecular weight counterparts. The BCP micelle core is formed by the solvophobic blocks, while the soluble blocks in the corona provide colloidal stability to the micelle. The thermodynamically-favored micelle morphology depends on the volume fraction of the solvophilic and solvophobic blocks, which is related to the molecular properties of the two blocks, namely their molar mass and chemical composition. It is affected also by the quality of the solvent for the solvophilic block and by the attraction of the two blocks towards each other.[2] When a solvent-selective BCP comprises two blocks miscible in the bulk phase, the attraction between the two blocks becomes an important parameter to consider when assessing its assembly in a selective solvent. We recently reported that poly(L-lactide)-*b*-poly(2-isopropyl-2-oxazoline) (PiPOx-*b*-PLLA) BCPs are miscible in the bulk.[3] Dipolar interactions of the carbonyl-groups of the PiPOx and PLA blocks are responsible for the miscibility, as confirmed experimentally in the FTIR spectra of PiPOx-*b*-PLLA, which presents shifts of the PiPOx carbonyl-stretching vibrations as a function of the PLLA content. The close values of the solubility parameters of PiPOx and PLA (δ_{PiPOx}: 24.0 $J^{0.5}/cm^{1.5}$, δ_{PLA}: 22.7 $J^{0.5}/cm^{1.5}$) calculated by the method of Fedors[4] support the experimental observations.

PiPOx is a semi-crystalline polymer soluble in polar organic solvents and in cold water. Its aqueous solutions undergo a phase transition upon heating, yielding a phase-separated turbid suspension from which PiPOx eventually crystallizes in the form of fibrillar nanostructures.[5] The phase transition temperature of aqueous PiPOx solutions markedly depends on the polymer molecular weight. The cloud point temperature (T_{CP}) of PiPOx in water (1 g/L) decreases from 73 °C to 36°C as the PiPOx molar mass (M_n) increases from 1.9 kg/mol to 16.7 kg/mol .[6,7] Oligo-PiPOx samples consisting of 6 repeating

units or fewer (M_n < 0.7 kg/mol) remain soluble in water beyond 80 °C.[8] Previously reported diblock copolymers consisting of a PiPOx block and a water-insoluble block were shown to associate in water in the form of core/corona nanoparticles with a core containing the hydrophobic blocks and a corona consisting of hydrated PiPOx chains. Upon heating the BCPs dispersions in water beyond their phase-transition temperature, a sharp increase of turbidity occurred, reflecting the cooperative dehydration of the PiPOx blocks and subsequent inter-particle aggregation. Examples of hydrophobic blocks employed include poly(ethylene), poly(2-(4-tert-butoxycarbonyl)amino)butyl-2-oxazoline) and poly(ferrocenyl-dimethylsilane).[9,10] Stoichiometric mixtures in water of two oppositely charged diblock ionomers, such as the PiPOx-*b*-poly(L-lysine)/PiPOx-*b*-poly(aspartic acid) pair, also assemble in water, forming core-corona polyion complex (PIC) micelles first reported by Kataoka.[11] Di-hydrophilic block copolymers are also of interest, in which the PiPOx block is linked to another water-soluble block,[12–16] which may be thermo-responsive.[17–21]

PLA is an approved material by the the food and drug administration (FDA) and used in various implants.[22–24] The monomer, lactide, has two asymmetric carbons. PLAs have different microstructures depending on the configuration of the monomer. Polymerization of (*S,S*)-lactide (L-lactide) yields isotactic PLLA, while the polymerizations of (*R,S*)-lactide (*meso*-lactide) or of a racemic mixture of (*R,R*)-lactide and (*S,S*)-lactide (DL-lactide) yield PDLLA of irregular microstructure. PLLA is semi-crystalline and less soluble in organic solvents than the amorphous PDLLA.[25] PLA in its various forms has been evaluated for use in injectable drug delivery formulations,[26] especially in the form of nanoparticles.[27,28]A number of drug delivery studies focused on micellar structures of diblock copolymers of PLA and poly(2-ethyl-2-oxazoline) (PEtOx), a lower homolog of PiPOx approved by FDA as indirect additive used in food contacting substances.[29–31] The calculated solubility parameter of PEtOx (δ_{PEtOx}: 25.7 $J^{0.5}/cm^{1.5}$) suggests that PEtOx and PLA are not miscible. Accordingly, PEtOx-*b*-

PLA copolymers were reported to form core/corona particles. Although PEtOx is thermo-responsive, the temperature dependent behavior of PEtOx-b-PLA in water has not been reported.

We examine here the self-assembly in water of PiPOx-*b*-PLA diblock copolymers (Scheme 1). Aware of the miscibility of PiPOx and PLA, we designed a comprehensive experimental approach to determine the morphology of PiPOx-*b*-PLA particles in aqueous dispersions at 25 °C and upon heating to 50 °C. ^{1}H-NMR spectroscopy, turbidimetry, high-sensitivity differential scanning calorimetry (HS-DSC), dynamic light scattering (DLS), and small angle neutron scattering (SANS) led us to conclude that a significant fraction of PiPOx is not exposed to water, but confined in close proximity to PLA blocks. We demonstrate that the precise particle morphology depends on the molecular weight of the PLA and PiPOx blocks and on the chirality of the PLA fragment.

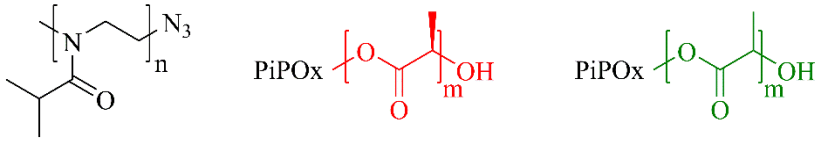

PiPOx PiPOx-b-PLLA PiPOx-b-PDLLA

Scheme 1 Chemical structures of PiPOx and the BCPs

Experimental:

Materials: De-ionized water (> 5 MΩcm) or deuterium oxide (D_2O, 99.96 % D, Euriso-top) and tetrahydrofuran (THF, > 99.9 %, inhibitor-free, Honeywell) were used without further purification. Dialysis units (Pur-A-Lyzer, molecular weight cut-off 3500 g/mol, Sigma-Aldrich) were washed in de-ionized water before use. The diblock copolymers PiPOx-*b*-PLA (Scheme 1 and Table 1, right) were prepared via click coupling of preformed azide-terminated PiPOx with propargyl-terminated PLA using the homopolymers listed in Table 1, left.[3]

Particle preparation: A PiPOx-*b*-PLA solution in THF (0.5 mL, 10 g/L) was added within one minute to de-ionized water (2.5 mL) stirred at 300 rpm using a syringe equipped with a needle of 0.4 mm diameter. At the end of the addition, the sample was stirred in air at room temperature for two hours to remove THF gradually by evaporation. The remaining dispersion was dialyzed against de-ionized water overnight. The dispersion was recovered and brought to a concentration of 0.5 g/L by addition of de-ionized water. The dispersion was passed successively through Nuclepore Track-Etch Polycarbonate Membrane of pore sizes of 400, 200 and 100 nm using an Avanti Polar Lipids miniextruder. The dispersion was passed 11 times through each membrane. The weight loss of polymer was less than 5 %, as determined gravimetrically. The particles are stable at room temperature for 10 days or longer (see SI2-1).

The same process was used to prepare samples for SANS measurements, starting with a PiPOx-b-PLA solution in THF (0.1 mL, 50 g/L) and D_2O (0.5 mL). After one hour of stirring in air, the dispersion was dialyzed against D_2O overnight, brought to a concentration of 5 g/L by addition of D_2O, and extruded as described above. For NMR analysis, dispersions were also prepared in D_2O and brought to a concentration of 25 g/L. They were not extruded.

For heat treatment, particle dispersions in H_2O (0.5 g/L) or D_2O (5 g/L) were freshly prepared as described and heated from room temperature to 50 °C with a rate of 1 °C/min. After keeping the temperature at 50 °C for 2 hours, the dispersions were cooled back to room temperature with a rate of 1 °C/min and analyzed by light scattering, SANS or cryo-TEM without further delay.

Proton nuclear magnetic resonance spectroscopy: ^{1}H-NMR spectra were recorded with a Bruker Avance III 500 spectrometer. Polymer solutions or dispersions in D_2O were used. The spectra were recorded at room temperature and normalized to the intensity of the HOD peak (4.8 ppm).

Light scattering: Dynamic (DLS) and static light scattering (SLS) measurements were performed with a setup consisting of a Brookhaven Instruments goniometer BIC-200SM, a BIC-TurboCorr digital auto/cross-correlator and a BIC-CrossCorr detector combining two BIC-DS1 detectors. The light source was a Coherent Sapphire 488-100 CDRH laser operating at a wavelength of 488 nm. The temperature was set to 20 °C. The hydrodynamic radius R_h was calculated according to Stokes-Einstein equation:

$$R_h = \frac{kT}{6\pi\eta D} \quad \text{(Equation 1)}$$

where k is the Boltzmann constant, T the absolute temperature, η the viscosity of the solvent, and D the mutual diffusion coefficient obtained by a linear fit of the decay rate Γ vs. the squared scattering vector q^2, with:

$$\Gamma = Dq^2 \quad \text{(Equation 2)}$$

$$q = \frac{4\pi n_0}{\lambda} sin\frac{\theta}{2} \quad \text{(Equation 3)}$$

where n_0 is the refractive index of the solvent, λ the wavelength of the laser, and θ the scattering angle. Γ is obtained from a second order cumulant expansion of the first-order electric field correlation function of the scattered electric field $g_1(t)$. Particle size and dispersity were analyzed also by the CONTIN algorithm (see SI3).

The averaged intensity of scattered light I_{sample} at θ was measured by SLS over 3 min, the accumulation time in the DLS experiment, and used to calculate the Rayleigh ratio of the sample R_Θ^{sample}.[32]

$$R_\theta^{sample} = (I_{sample} - I_{solvent}) \frac{R_{tol}}{I_{tol}} \quad \text{(Equation 4)}$$

where $I_{solvent}$ and I_{tol} are the scattered light intensities of the pure solvent and toluene at 90°, respectively, and R_{tol} the Rayleigh ratio of toluene. For a precise extrapolation of R_Θ^{sample} to Θ = 0°, measurements were conducted at 11 angles between 50° and 150°. The resulting form factor P(Θ) was fitted to a Guinier model to obtain the radius of gyration R_g.

$$P(\Theta) = \frac{R_\Theta}{R_{\Theta=0}} = \exp\left(-\frac{q^2}{3}\langle R_g^2\rangle\right) \quad \text{(Equation 5)}$$

Small angle neutron scattering: SANS measurements were carried out at the JEEP II reactor at IFE, Kjeller. The wavelength was set with the aid of a velocity selector (Dornier), using a wavelength resolution $\Delta\lambda/\lambda$= 10%. Two different detector distances (1.0 to 3.4 m) and two wavelengths (5.1 Å and 10.2 Å) were employed to obtain a wave-vector range from 0.007 to 0.32 $Å^{-1}$. Here q, the absolute value of the wave-vector, is given by:

$$q = (4\pi/\lambda)\sin(\theta) \quad \text{(Equation 6)}$$

where θ is the scattering angle. The samples were kept in 2 mm quartz cuvettes, equipped with stoppers. The measuring cells were placed onto a copper base for good thermal contact before mounting in the sample chamber. Samples were kept at a temperature of 25 °C. The transmission was measured separately. The absolute scattering cross section (cm^{-1}) was calculated by taking into account the contribution from the empty cell and the general background. The samples were prepared in D_2O instead of H_2O to enhance contrast and reduce incoherent background.

The size of non-interacting moieties was determined in terms of the radius of gyration (R_g) at small q-values through the Guinier expression for the scattered intensity (I(q)):

$$\ln I(q) = lnI(0) - \frac{1}{3}q^2R_g^2 \quad \text{(Equation 7)}$$

This approximation is valid only for $qR_g < 1$. Since the Guinier approximation yielded quite coarse fits of the data, we also made full model fits of the scattering curve:

$$I(q) = \frac{N}{V}P(q)S(q) \quad \text{(Equation 8)}$$

where N is the number of particles inside a sample volume V, P(q) the particle form factor, and S(q) the particle structure factor. Since the particle dispersions used here are quite dilute we can assume non-

interacting particles and for this case $S(q)=1$. The form factor of homogenous spherical objects with a radius R can be written as:

$$P(q) = (\Delta\rho)^2 V_p^2 \left[\frac{3}{(qR)^3}\{\sin(qR) - qR\cos(qR)\}\right]^2 \quad \text{(Equation 9)}$$

where $\Delta\rho = \rho_p - \rho_0$ is the difference in scattering length density (SLD) between particle and solvent (scattering contrast) and V_p is the particle volume. In the fitting of the SANS data, we generally found this model adequate for the samples measured before heating. However, in one case it was necessary to employ the spherical core-shell model given by

$$P(q) = \frac{scale}{V_s}\left[\frac{3V_c(\rho_c-\rho_s)j_1(qR_c)}{qR_c} + \frac{3V_s(\rho_s-\rho_0)j_1(qR_s)}{qR_s}\right]^2 \quad \text{(Equation 10)}$$

where V_s is the total particle volume (including the shell), V_c is the volume of the core, R_s is the radius of the shell, and R_c is the radius of the core, thus $R_s = R_c + d$, where d is the thickness of the shell. The parameter ρ_c is the scattering length density of the core and ρ_s is the scattering length density of the shell. $j_1(x) = (\sin x - x \cos x)/ x^2$, and *scale* is a scale factor proportional to the sample concentration.

Some of the samples were best described by a cylinder model after heating. The core-shell cylinder model for overall random particle orientation has a form factor $P(q)$ described by:

$$P(q) = \frac{scale}{V_s}\int_0^{\frac{\pi}{2}} f^2(q,\alpha)\sin\alpha \, d\alpha \quad \text{(Equation 11)}$$

with

$$f(q,\alpha) = 2(\rho_c - \rho_s)V_c j_0(qH\cos\alpha)\frac{J_1(qR_c\sin\alpha)}{qR_c\sin\alpha} + 2(\rho_s - \rho_{solv})V_s j_0[q(H+t)\cos\alpha]\frac{J_1(qR_s\sin\alpha)}{qR_s\sin\alpha}$$

(Equation 12)

Here, α is the angle between the axis of the cylinder and the q-vector, V_c and V_s are the core volume and total volume, as before. Thus, for the cylinder $V_c = \pi R_c^2 L$ and $V_s = \pi R_s^2 L$, where L is the length of the

core, R_c is the radius of the core, and t is the thickness of the shell ($R_s = R_c + t$). The total length of the outer shell is given by $L+2t$. J_1 is the first order Bessel function, and $j_0(x) = \sin x / x$.

The scattering length densities employed in this study are 1.73e-06 Å^{-2} for PLA[33] and 0.7e-06 Å^{-2} for PiPOx. The model fitting was implemented via the SasView analysis package (http://www.sasview.org/).

Wide angle X-ray scattering: WAXs measurements were conducted with a system consisting of a generator (Seifert, 36 kV, 25 mA), a conventional sealed X-ray tube (PANalytical), a Montel multilayer monochromator and a 2-dimensional Mar345 image plate detector (Marresearch GmbH) operating in a perpendicular transmission geometry. The selected wavelength was CuKα, 1.541 Å. Dispersions before and after treatment at 50 ºC were freeze-dried. The powders obtained were placed between two Mylar foils separated with an aluminum ring used as frame.

Transmission electron microscopy: TEM measurements were performed on a Hitachi FESEM S-4800 electron microscope. Samples for imaging were prepared by placing a drop of dispersion (0.5 g/L) on a 300 mesh Cu grid and air-drying. Cryo-TEM observations were carried out with a FEI Talos Arctica microscope operated at 200 kV. Dispersions (0.5 g/L, 3 µL aliquots) were vitrified with a Leica EMGP vitrification device using freshly glow-discharged Quantifoil R1.2/1.3 grids. Images were recorded at a 57,000× magnification with a FEI Falcon 3 camera operated in the linear mode.

Turbidimetry: Changes with temperature of the transmittance at 400 nm of a particle dispersion were recorded on a JASCO J-815 CD spectrometer equipped with a PTC-423S/15 Peltier type temperature control system. Samples were heated from 20 to 80 °C at a heating rate of 1 °C/min. The sample temperature was measured via a thermocouple placed in the dispersion throughout the measurement.

High sensitivity differential scanning calorimetry: Thermograms were obtained with a Microcal VP-DSC micro-calorimeter. Degassed dispersions (0.5 g/L) were added to the sample cell (0.52 mL) and

measurements were performed at an external pressure of ca. 180 kPa. After an equilibration time of 30 min at 10 °C, the sample was heated once to 80 °C at a heating rate of 1 °C/min.

Results and Discussion:

General considerations. The diblock copolymers were prepared by click ligation of an azide-terminated poly(2-isopropyl-2-oxazoline) and a propargyl-terminated poly(lactide). The molecular characteristics of the homopolymers, PiPOx, PLLA, and PDLLA are presented on the left-hand side of Table 1. On the right-hand side of Table 1, we give the composition and molar mass of 10 diblock copolymers prepared by click coupling of the homopolymers listed on the left-hand side of Table 1. The PiPOx-*b*-PLAs are organized in two subsections (entries 1-6 and 7-10) according to the molecular weight of the PiPOx block. Within each subsection, the copolymers containing PLLA are listed first, followed by those containing a PDLLA block. The composition of four diblock copolymers studied in detail in this report is printed in bold font in Table 1. The other samples were used for specific measurements to identify trends and strengthen the validity of the mechanisms proposed. We prepared this large sample set, in order to assess the dependence of the BCPs self-assembly in water on the BCPs chemical composition, molar mass, and the lactide chirality.

The dispersions were prepared at room temperature by rapid addition into deionized water of a concentrated solution of the BCPs in THF, a good solvent for all copolymers. The copolymers associate in water/THF mixtures of water content above a given value that depends markedly on the stereochemistry and molecular weight of the PLA block (see SI 1-1).

Table 1 Molecular properties of the polymers investigated taken from reference [3]

Homopolymers			*Diblock copolymers*			
Name[a]	$M_n^{GPC,b}$	PD^{GPC}	Name[c]	$M_n^{NMR,d}$	$\Phi^{PiPOx,e}$	n/m^f
PLLA1	5.9	1.11	2L1	9.5	66	1.9
PLLA2	10.0	1.09	**2L2**	**11.6**	**50**	**1.0**
PLLA3	14.6	1.06	2L3	14.9	37	0.6
PDLLA1	4.9	1.43	**2DL1**	**11.1**	**53**	**1.1**
PDLLA2	9.0	1.41	2DL2	14.3	39	0.6
PDLLA3	17.7	1.35	2DL3	19.8	26	0.4
PiPOx2	9.3	1.10	3L1	15.3	74	2.8
PiPOx3	15.5	1.28	**3L3**	**20.2**	**51**	**1.0**
			3DL1	16.7	65	1.9
			3DL3	**25.6**	**38**	**0.6**

[a] Nomenclature of homopolymers adopted from reference [3]; [b] in kg/mol, PS calibration, THF as eluent; [c] Nomenclature block copolymers: "2L1" = "PiPOx2-b-PLLA1"; [d] absolute molecular weight in kg/mol, calculated by relating M_n^{MALDI} (PiPOx2: 7.1 kg/mol, PiPOx3: 12.5 kg/mol) to the ratio of monomeric units obtained from ^{1}H-NMR spectra of the diblocks; [e] mol % PiPOx; [f] ratio n^{PiPOx}/m^{PLA} of monomeric units in the BCPs as defined in Scheme 1.

^{1}H-NMR spectroscopy analysis of aqueous copolymer dispersions at room temperature. In Figure 1, we present ^{1}H-NMR spectra of PiPOx2 in D_2O (black trace) and dispersions in D_2O of two PiPOx-b-PLA copolymers, 2L2 and 3DL3. The three lower spectra are normalized to the HOD signal at 4.8 ppm. The ^{1}H-NMR spectrum of PiPOx2 presents three characteristic signals at ~ 3.5, 2.8 and 1.1 ppm due to the resonances of protons C, B, and A (Figure 1). The intensity of the three signals is reduced significantly in the spectra of 2L2 and 3DL3. Based on the nominal concentration of PiPOx in the copolymer dispersions, we estimate that the signal around 3.5 ppm (-C*H*$_2$-C*H*$_2$-N-)$_n$ is reduced by factors of 400 and 150 in the spectra of 2L2 and 3DL3, respectively, compared to the PiPOx solution. The signals due to the protons of the hydrophobic PLLA and PDLLA blocks of 2L2 and 3DL3, expected to appear around 5.2 ppm (-CH-) and 1.6 ppm (-CH_3), cannot be detected at all, which indicates that the mobility of PLA chains within the nanoparticles is limited.

^{1}H-NMR spectra of typical PLA-containing core-shell nanoparticles do not present signals due to the PLA blocks, confined in the core of the micelles. However, they feature intense signals due to protons

of the solvophilic blocks since they retain their mobility in the corona where they are surrounded by solvent molecules. The corona block signals may broaden slightly, but their intensity is hardly affected, as reported for instance in the case of the related PLA-b-PEG particles dispersed in D_2O.[34,35] The fact that the PiPOx protons signals are very weak in the spectra of 2L2 and 3DL3 implies that the PiPOx and PLA chains coexist intermixed via dipole/dipole interactions through most of the particle volume. The residual PiPOx signals in the ^{1}H-NMR spectra 2L2 and 3DL3 may be due to residual mobile hydrated PiPOx chains, presumably located near the water/particle interface.

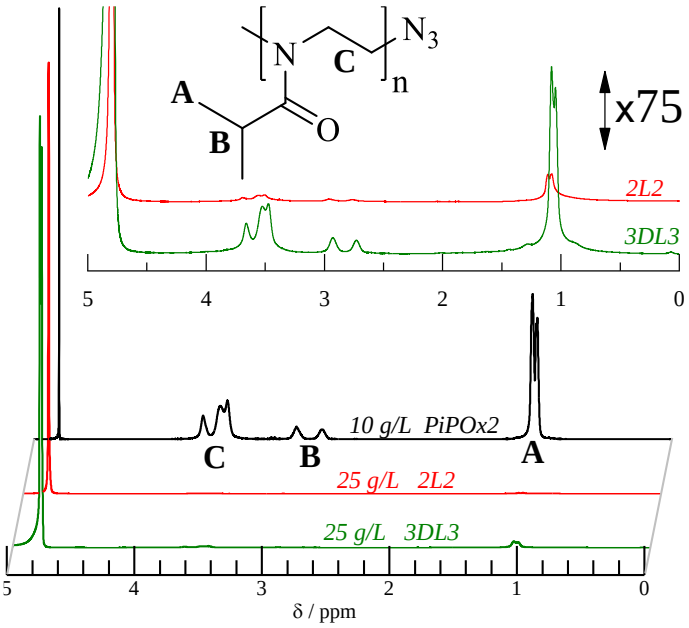

Figure 1 ^{1}H-NMR spectra of dispersions of 2L2 (25 g/L) and 3DL3 (25 g/L) in D_2O. The spectrum (black trace) towards the back of the Figure corresponds to a solution of PiPOx2 (10 g/L) in D_2O. Spectra are normalized to the intensity of the HOD signal (δ 4.8 ppm). Intensity-enhanced spectra (x75) of 2L2 and 3DL3 dispersions are shown in the top section of the Figure, together with the structure of the PiPOx monomer unit.

High-sensitivity-DSC and turbidimetry. Four PiPOx-b-PLA dispersions, 2L2, 3L3, 2DL1 and 3DL3, were analyzed by turbidimetry and microcalorimetry. Solutions of the PiPOx homopolymers used to prepare the BCPs were evaluated as well. The BCPs 2L2 and 3L3 differ in terms of their total molar mass (11.6 kg/mol vs 20.2 kg/mol) but for each BCP the number of PLA repeat units is nearly the same as the number of PiPOx units (see Table 1). The BCPs 2DL1 and 3DL3 contain DL-lactide. They differ in their total molar mass (11.1 kg/mol vs 25.6 kg/mol), and in the ratio of PiPOx monomer units to PDLLA repeat units. In all experiments, solutions were heated from 20 °C to 80 °C (with a rate of 1 °C/min) and cooled back to 20 °C with the same rate.

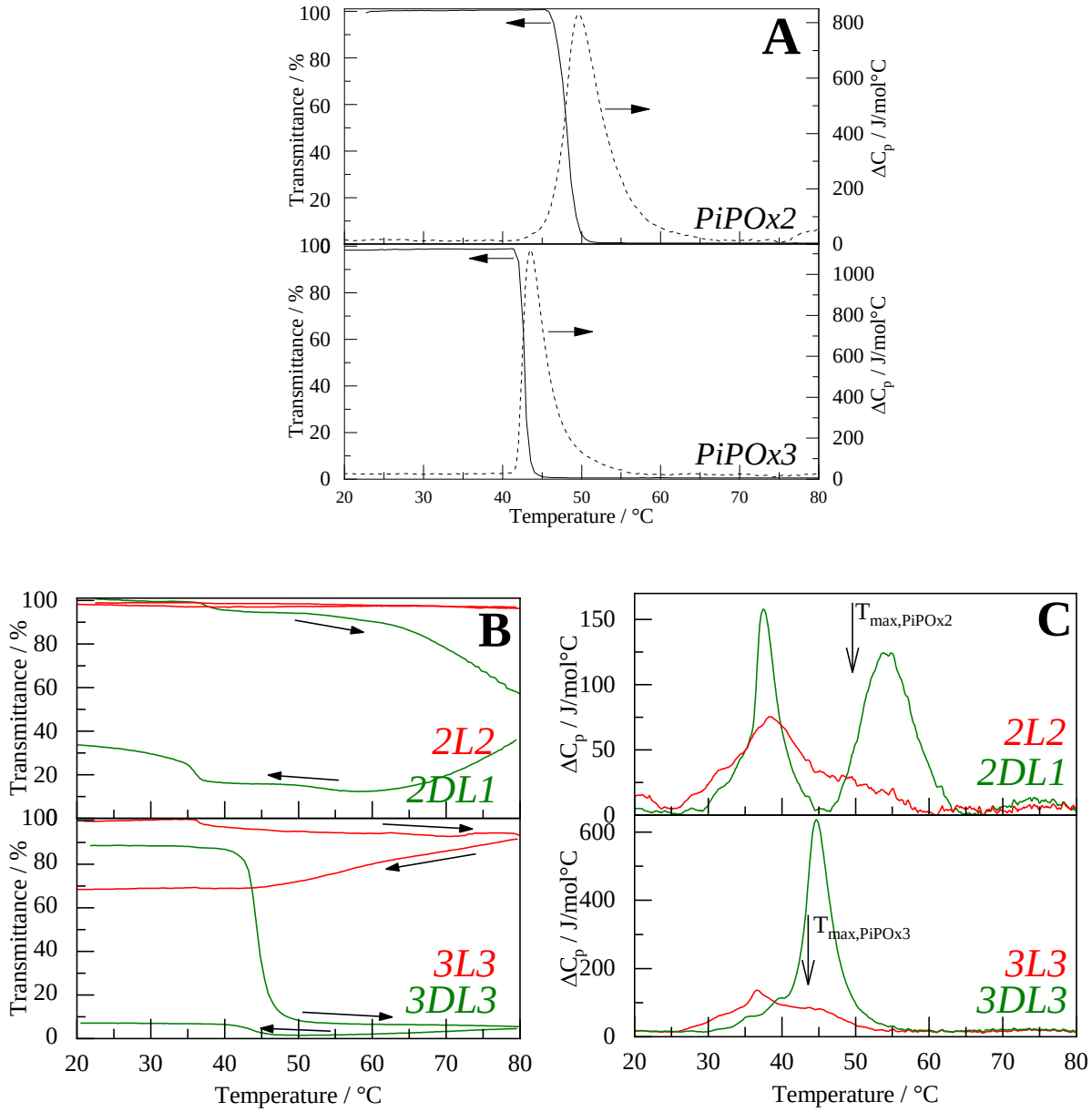

Figure 2 (A) Changes as a function of temperature in the transmittance and heat capacity upon heating of PiPOx2 and PiPOx3 aqueous solutions (polymer concentration: 0.3 g/L). (B) Changes as a function of temperature of the transmittance of 2L2, 2DL1, 3L3, and 3DL3 aqueous dispersions (polymer concentration: 0.5 g/L). The arrows follow the traces recorded upon heating and cooling. (C) Changes with temperature of the heat capacity of 2L2, 2DL1, 3L3, and 3DL3 aqueous dispersions upon heating.

Note the difference in the y-scales of the top and bottom panels. The arrows indicate the T_{max} of the corresponding PiPOx solutions (from Figure 2A).

Table 2 Thermal properties of PiPOx solutions and PiPOx-*b*-PLA dispersions in water

	Polymer	c_{PiPOx}[a]	T_{CP}[b]	$T_{max,1}$[c]	$T_{max,2}$[c]	ΔH_1[d]	ΔH_2[d]
Solutions	PiPOx2	0.30	45.9	-	49.6	-	4.8
	PiPOx3	0.30	41.4	-	43.6	-	4.8
Dispersions	2L2	0.31	-	38.4	48.8	0.8	
	3L3	0.31	-	36.6	45.0	1.4	
	2DL1	0.32	-	37.4	53.5	0.6	0.9
	3DL3	0.25	42.7	39.1	44.7	3.5	

[a] in g/L, nominal PiPOx concentration in the solution, [b] in °C, cloud point temperature from turbidimetry, [c] in °C, temperature at the maximum of a transition in HS-DSC, [d] in kJ/mol, transition enthalpy with an error margin of ± 0.1 kJ/mol.

a) Homopolymer solutions (Figure 2 A and Table 2). The cloud points of aqueous PiPOx2 and PiPOx3 solutions determined by the onset of turbidimetry are 45.9 °C and 41.4 °C, respectively. The corresponding endotherms measured by HS-DSC are unimodal (Figure 2 A, dashed lines). For both polymers, the onset of the endotherm coincides with the appearance of turbidity, an indication that the polymers dehydration is coupled to their aggregation. The enthalpy of the phase transition (4.8 kJ/mol) is the same for the two polymers and similar to reported values.[6] The endotherm is wider in the case of PIPOx2, compared to PiPOx3, which indicates that the cooperativity of the dehydration is less pronounced in the former case.

b) Dispersions of 3L3 and 2L2 (Figure 2 B and C, red curves). The transmittance of the 3L3 dispersion hardly changes over the 20 °C to 80 °C temperature range: it remains constant (near 100 %) up to 36 °C, then it decreases monotonously with increasing temperature, reaching a value of ~ 90 % at 80 °C. It continues to decrease upon cooling and eventually stabilizes around 70 % for T < 45.0 °C. The dispersion never recovers its original transmittance, even upon prolonged storage at room temperature (Figure 2B,

red traces). The endotherm of the 3L3 dispersion is broad, from 25 to 50 °C. It features a weak maximum at 36.6 °C ($T_{max,1}$) and a shoulder at 45.0 °C, a temperature close to the T_{max} of the PiPOx3 solution (Table 2). The transition enthalpy, calculated based on the total concentration of iPOx units in solution (2.7 mM), is 1.4 kJ/mol. From this transition enthalpy values, we estimate that ~ 30 % of the PiPOx of the 3L3 dispersion dehydrate upon heating. The HS-DSC and turbidity results are consistent with a 3L3 particle morphology whereby the PiPOx and PLA units of the two blocks form interblock complexes throughout the particles, leaving only a few short tails and loops of PiPOx on the particle outer surface. Short PiPOx oligomers units dehydrate only at high temperature and may remain hydrated up to 80 °C. The presence of short hydrated PiPOx oligomers may account for the colloidal stability of the 3L3 dispersion up to 80 °C. The small endotherm centered around 36.6 °C is attributed tentatively to the release of water molecules bound to the PiPOx chains confined in the PLA/PiPOx network, by analogy with the dehydration on dense PNIPAM brushes grafted to the surface of gold nanoparticles.[36] Such transitions were observed also in the study of star-like micelles formed by hydrophobically end-capped C_{18}-PiPOx-OH (10 kg/mol)[37] and attributed to the release of water from dense polymer brushes.

The response of 2L2 dispersions to changes in temperature (Figure 2B and 2C, red lines) is similar to that of 3L3 dispersions. The transition range and $T_{max,1}$ of the two samples are comparable (Table 2). The total enthalpy of the process is lower (0.8 kJ/mol, equivalent to 17 % of PiPOx) in the case of 2L2, compared to 3L3 and the shoulder on the higher temperature side, centered near T_{max} of the PiPOx2 solution, is less pronounced. The transmittance of 2L2 dispersions hardly changed over the entire heating/cooling scan, which we attribute to the low fraction of PiPOx chains that dehydrate at high temperature (Figure 2 B).

c) Dispersions of 2DL1 and 3DL3 (Figure 2 B and C, green curves): The HS-DSC trace of a 2DL1 dispersion exhibits two well-separated endotherms, with $T_{max,1}$ at 37.4 °C (0.6 kJ/mol) and $T_{max,2}$ at 53.5 °C (0.9 kJ/mol). The total transition enthalpy is similar to that recorded for a 3L3 dispersion. The transmittance of a 2DL1 dispersion decreases slightly, from 100 to 95 %, around 36.7 °C, remains constant upon heating up to 52 °C, and decreases to reach a value of ~ 60% at 80 °C. It decreases further upon cooling, reaching a minimum (12 %) at 60 °C. The transmittance of the dispersion kept at 25 °C, remains constant (34 %).

The fact that the 3DL3 dispersion remains turbid upon cooling is surprising. It implies that the 3DL3 aggregation that occurs at high temperature is not reversible. The thermogram of the 3DL3 dispersion (Figure 2C, bottom) presents a single endotherm with T_m = 44.7 °C and an enthalpy of 3.5 kJ/mol. These features indicate that 3DL3 particles prior to heat treatment adopt a morphology akin to a core/corona morphology. Given the low enthalpy of the transition, the core of the particles cannot consist of PLA alone, but must contain complexed PLA and PiPOx blocks.

Light scattering of dispersions at room temperature. The hydrodynamic size of the BCP particles in aqueous dispersions at room temperature was determined by DLS. Autocorrelation functions were analyzed by a second order cumulant fit to extract the decay rates Γ between 50 and 150 °. Plots of Γ vs the squared scattering vector q for 2L2, 3L3, 2DL1 and 3DL3 are displayed in Figure 3, together with CONTIN plots at a scattering angle of 90 °. See Figure S3-1 for Γ vs q^2 plots of the remaining samples. All Γ vs q^2 plots were linear, which confirms translational diffusion of the nanoparticles. The R_h of the particles increases with the molar mass of the BCPs, from 18 nm for 2DL1 to 60 nm for 3DL3.

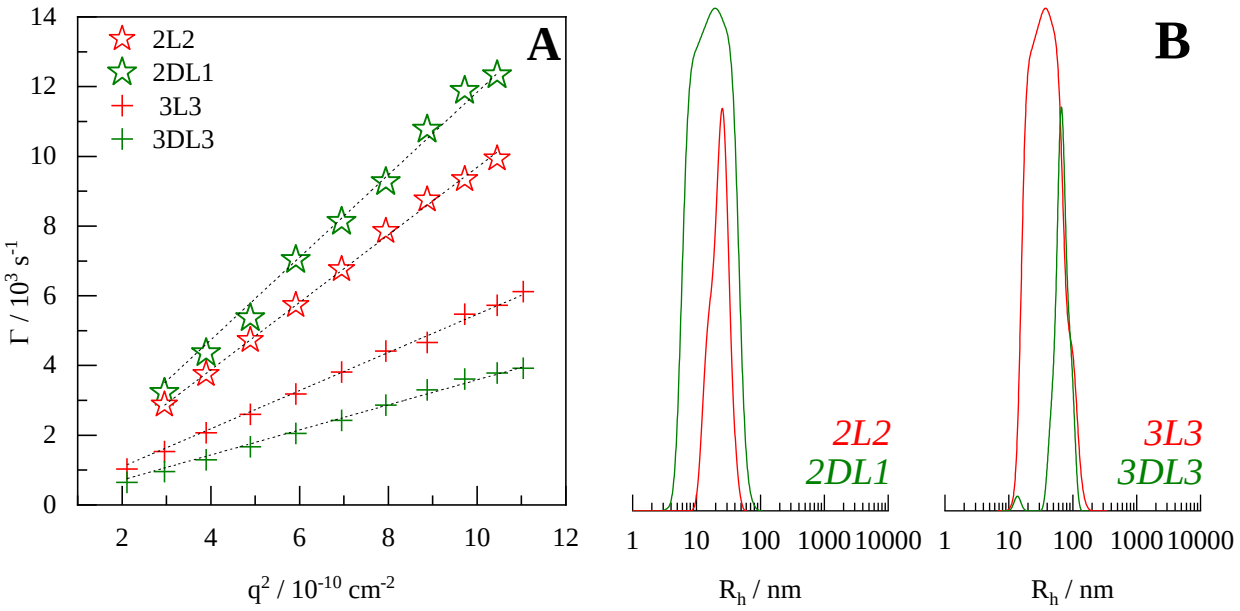

Figure 3 (A) Decay rates Γ from second order cumulant analysis vs squared scattering vector q. The dashed lines are linear fits according to $\Gamma = Dq^2$. (B) CONTIN plots at 90 ° of the corresponding dispersions.

The radii of gyration (R_g) (Table 3) of the particles were obtained by a Guinier fit of the corresponding form factor functions, P(Θ), obtained from the average intensity of scattered light measured by SLS. The dimensionless parameter $\rho = \frac{R_g}{R_h}$, which reflects the mass distribution of the scattering object, is an indicator of the morphology of nanoparticles and of single chain conformation.[38] The values of the ρ-parameter vary from 0.9 to 1.1 for all of the BCPs dispersions, except 2DL1 (Table 3). This range of ρ-values encompasses 0.926, the ρ-value predicted for collapsed globes, fully permeable to the solvent and with uniform segment distribution.[39] The fact that the ρ-parameter does not change over a wide range of BCP molecular characteristics is quite remarkable, considering that the molar fraction of the PiPOx units changes by a factor of 3 and the solubility properties of PLLA and PDLLA are entirely different.[39] For core/corona particles, such a large change of the hydrophilic block fraction is accompanied by significant changes in the extent and density of the corona detectable through the evolution of the ρ-parameter. In

the case of the 2DL1 dispersion, the ρ-parameter reaches 1.6. This point is addressed in relation to SANS data presented in the following section.

Table 3 Particle sizes of PiPOx-b-PLA dispersions measured by light scattering and SANS at 20 °C. The samples were first measured as prepared and second after keeping at 50 °C for two hours. The bold entries are discussed in the text in more detail.

	As prepared				*After 2 h at 50 °C*			
Name	R_h[a]	R_g[b]	R_g/R_h	R^{SANS}	R_h[a]	R_g[b]	R_g/R_h	R^{SANS}
2L1	19	20	1.0	-	-	-	-	-
2L2	**22**	**25**	**1.1**	**15.1**	**24**	**24**	**1.0**	**15.3**
2L3	28	31	1.1	-	-	-	-	-
2DL1	**18**	**29**	**1.6**	**9.9**	**bimodal**			**9.2**
2DL2	29	28	0.9	-	-	-	-	-
2DL3	39	39*	1.0	-	-	-	-	-
3L1	22	22	1.0	-	-	-	-	-
3L3	**39**	**42**	**1.1**	**17.5**[c]	**bimodal**			**16.1**[c]
3DL1	25	28	1.1	-	-	-	-	-
3DL3	**60**	**65***	**1.1**	**17.3**	**bimodal**			**14.0**

All radii are given in nm; [a] Hydrodynamic radius R_h is obtained by the linear fit to the data presented in Figure 2. [b] Radius of gyration R_g is obtained by a fit of first or second order (marked with an *) to the ln[P(q)] vs q^2 data presented in the SI. [c] core-shell model with 12.0 nm core and 5.5 nm shell before heating and 13.3 nm core and 2.8 nm shell after heating

SANS of dispersions at room temperature. Measurements were carried on dispersions in D_2O of 2L2, 3L3, 2DL1, and 3DL3

a) Dispersions of 2L2 and 3L3 (Figures 4 A and B): The SANS data collected for the 2L2 dispersion were fitted with a sphere model of homogeneous density (Figure 4 A), yielding a particle radius, $R_{SANS,}$ of 15.1 nm. A model-independent Guinier fit led to $R_{g,SANS}$ = 14.8 nm. In the case of the 3L3 dispersion, SANS data (Figure 4 B) were best fitted with a core-shell model, yielding a particle radius of 17.5 nm and core radius of 12 nm, respectively. The scattering length density (SLD) of the core was initially set to the pre-calculated value for an averaged PLA/PIPOx complex (1.21e-06 $Å^{-2}$). It could be fitted to a value slightly higher than that (1.36e-06 $Å^{-2}$), indicating a near homogeneous mixture of PLA and PiPOx in the core with just a slight dominance of PLA. However, it should be noted that the overall fit is not

very sensitive to the core SLD-value, so that the uncertainty in the value quoted above is relatively large (ca. ±0.2 e-06 $Å^{-2}$). The SANS-derived radius of both 2L2 and 3L3 are smaller than their hydrodynamic sizes obtained by DLS (Table 3). This likely results from the low neutron scattering contrast of hydrated regions of the particles, showing that the corona is highly diluted and/or not well developed. The fact that 2L2 and 3L3 particles appear similar in size in SANS indicates that the contrast is lost abruptly at a distance from the center of around 15 - 18 nm. The diffusion-based R_h-value obtained by DLS is very sensitive to the hydrated regions and the values for the two samples are very different (R_h: 22 and 39 nm, respectively). This may indicate that the longer PiPOx3 tails extend further in the continuous phase than the shorter PiPOx2 chains.

b) Dispersions of 2DL1 and 3DL3 (Figures 4 C and D): 2DL1 is the PDLLA-analog to 2L2 in terms of PiPOx mol fraction. The SANS data of 2DL1 fitted with a homogeneous sphere model yielded R_{SANS} = 9.9 nm (Figure 4 C). This low value may indicate a high degree of particle hydration, which enhances the contrast problem of SANS and is consistent with the much higher ρ-parameter (1.6) of 2DL1, compared to the other samples. The radius of gyration of 2DL1 obtained by light scattering is larger by a factor of 2.9 than R_{SANS} (Table 3). Thus, both light scattering and SANS argue for a loose and highly hydrated PDLLA/PiPOx complex in the 2DL1 particle core in comparison to the rather dense PLLA/PiPOx complex of 2L2. In the 3DL3 sample the PiPOx mol fraction (38 %) is lower than in the other examples discussed. The size of 3DL3 particles derived from SANS data using a homogeneous sphere model fit is R_{SANS} = 17.3 nm, (Figure 4 D). Light scattering of the 3DL3 dispersion yields significantly larger sizes than SANS (by a factor of 3.8), indicating that long hydrated PiPOx tails extend form the particles into the surrounding aqueous phase.

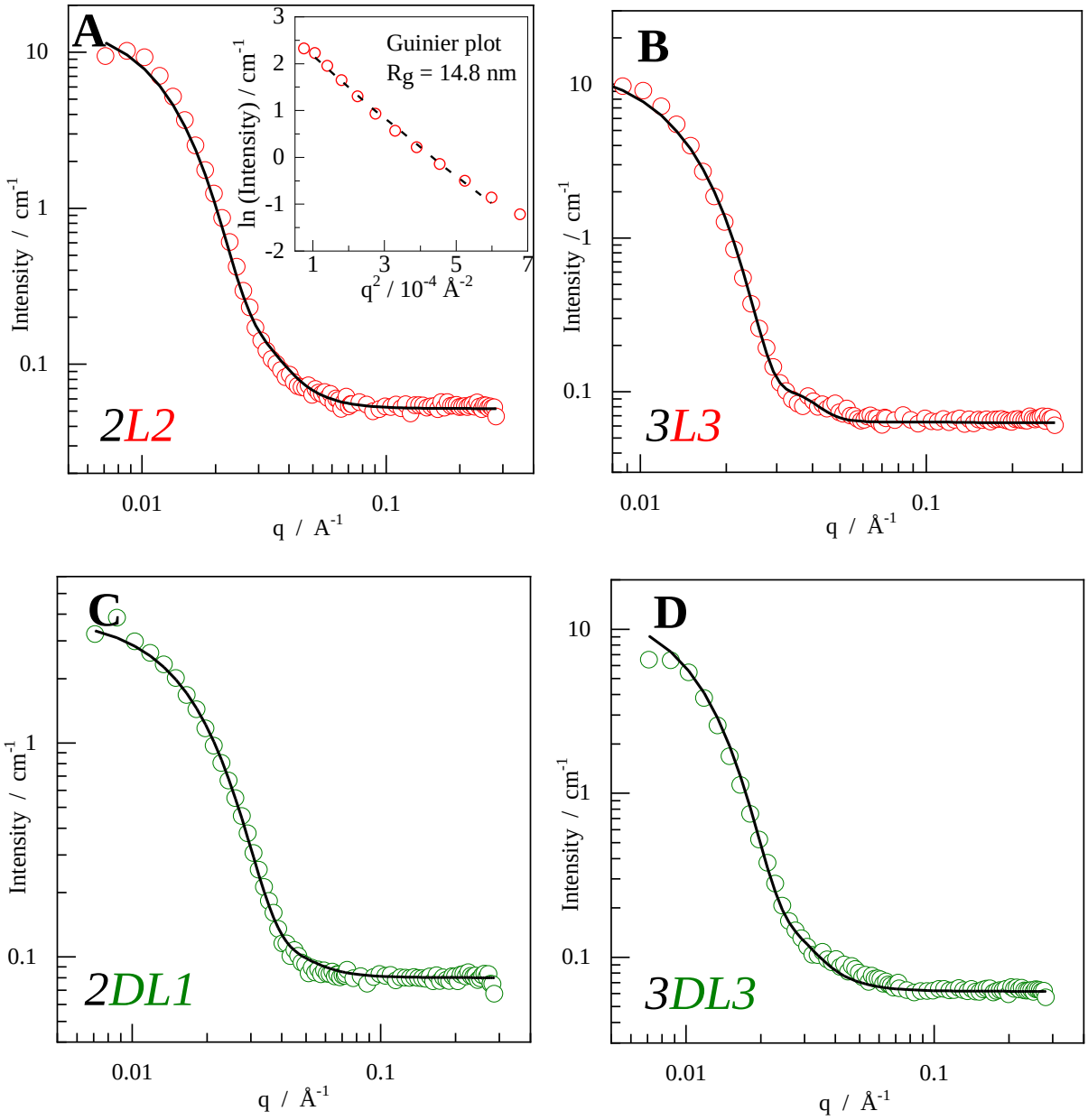

Figure 4 SANS data of the PiPOx-*b*-PLA dispersions (5 g/L, D_2O) directly after preparation measured at 20 °C. The lines are fits to the models described in the text. The inset in (A) shows a Guinier plot.

Cryo-TEM observations. A 3L3 dispersion in water was vitrified and observed by cryo-TEM. The micrograph (Figure 5) presents diffuse spherical objects of low contrast having an average radius of 8.7

± 1.4 nm, a value smaller than the core size obtained by SANS (12 nm). Both cryo-TEM and SANS are sensitive to contrast variations. Cryo-TEM "sees" the electronic density of the object while the SANS contrast varies with the hydration level. The spheres are distributed on the micrograph background at regular intervals, which suggests that prior to vitrification the dispersed 3L3 particles repelled each other by steric interactions. The distance between the centers of contiguous spheres in the micrograph is ~ 70 ± 10 nm, or approximately twice the R_h of the 3L3 particles determined by DLS (39 nm).

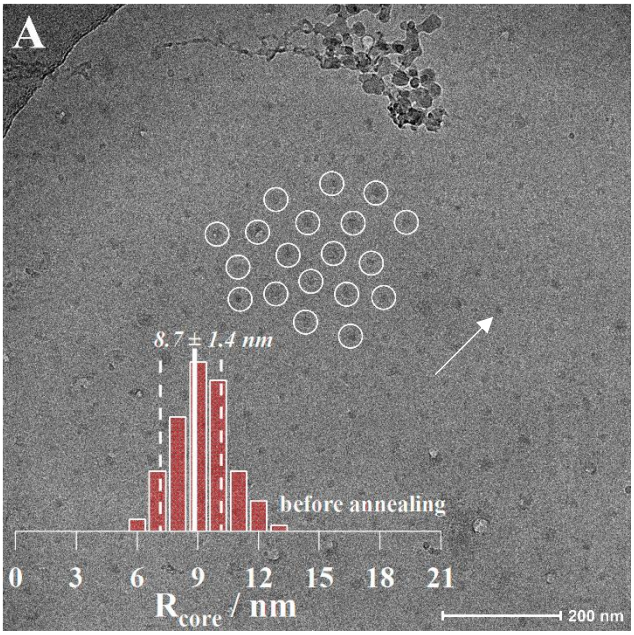

Figure 5 Cryo-TEM image of the 3L3 dispersion vitrified at room temperature immediately after preparation. The inset shows the core radius distribution and the white circles are a guide for the eye to estimate the particle distance. The arrow points to the core of a particle.

Tentative morphology of particles in aqueous dispersions at room temperature (Scheme 2). Taken together the results presented so far indicate that the particles consist of a core of associated PLA and PiPOx chains held together via dipole/dipole interactions. The core is surrounded by tethered hydrated PiPOx chains that extend in the aqueous continuous phase. The 3L3 particles consist of a dense core, a hydrated transition region (the shell in the SANS model) and a corona of PiPOx tails extended into the

water phase. The hydrodynamic sizes of 2L2 and 3L3 are significantly different, but their ρ-parameters are identical, indicating structural similarities. By SANS, the overall radii of 2L2 and 3L3 are comparable, but 2L2 is best fitted with a homogenous sphere model, whereas in the case of 3L3 a core-shell model gave a better fit. The more compact, less hydrated, morphology of the core of the 3L3 particles may reflect the lower solubility of PLLA3 in water, compared to PLLA2. The discrepancy between the R_{SANS} and R_h reflects differences in the sensitivity of SANS and DLS towards the outermost parts of the particles. In conclusion, the corona layer of the 2L2 is comparably thin. The main difference between the PLLA- and PDLLA-containing particles is the lower density/ higher degree of solvation of the PiPOx/PDLLA complex in the core. This results in higher particle elasticity.

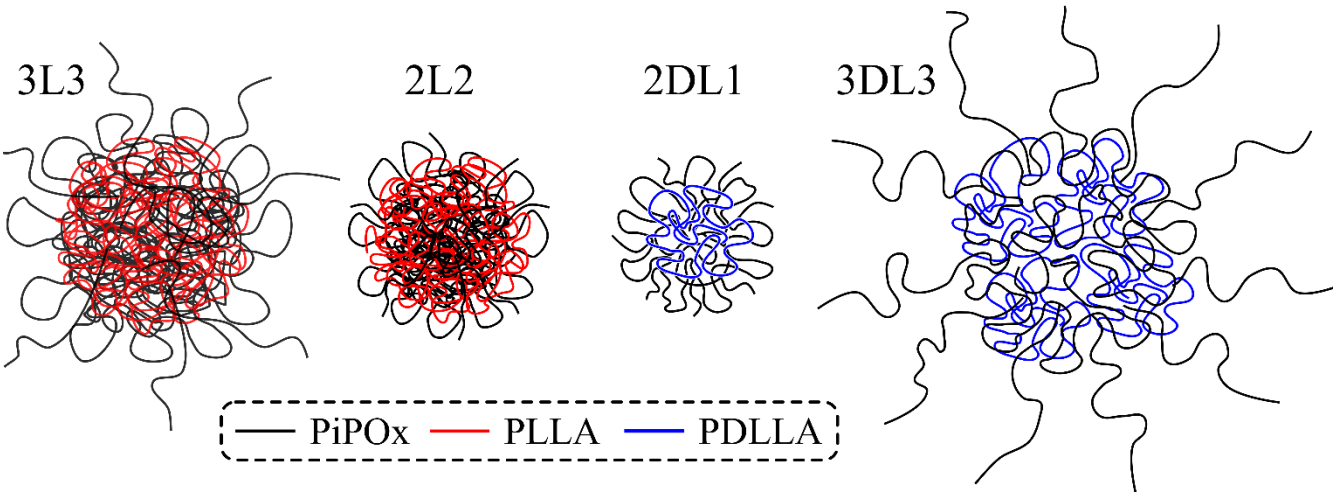

Scheme 2 Schematic illustration of the particle structures formed by 3L3, 2L2, 3DL3 and 2DL1. For a detailed description see text.

Temperature-dependent properties of PiPOx-b-PLA aqueous dispersions. Turbidity measurements of dispersions of 3L3, 2DL1 and 3DL3 in water (Figure 2B) indicated that originally clear dispersions become turbid upon heating and remained turbid upon cooling, unlike the dispersion of 2L2. The high elasticity of the PDLLA containing particles and the larger extension of the corona layer of the 3L3

particles inferred by the SANS data suggests that these particles coagulate upon heating. A set of temperature-dependent experiments were performed to test this hypothesis. Dispersions of 3L3 (0.5 g/L) were heated from 20 °C to 51 °C and monitored by DLS at 42 °C, i.e. above $T_{max,1}$ but below $T_{max,2}$ (HS-DSC), and at 51 °C. Subsequently they were cooled to 20 °C, and tested again. CONTIN plots at a 60 ° scattering angle are displayed in Figure 6. The R_h of the particles initially decreases, from 49 nm (20 °C) to 40 nm (42 °C). A bimodal distribution of particles (R_h ~ 30 and 200 nm) is detected at 51 °C. The dispersion remained bimodal upon cooling to 20 °C, with distributions of ~ R_h 45 nm and 420 nm. This indicates that a fraction of the rehydrated isolated particles is recovered, but a significant fraction of the large assemblies formed at 50 °C do not disassemble upon cooling. It would appear that the original particles coagulate into larger objects, which resist disintegration upon cooling and rehydration of the PiPOx chains. Bimodal distributions were also observed by DLS measurements at 20 °C after keeping the dispersions of 3L3, 2DL1 and 3DL3 at 50 °C for 2 hours (Table 3 and SI 3). In contrast, when the 2L2 dispersion was treated in the same way, no change in the particle size distribution was observed.

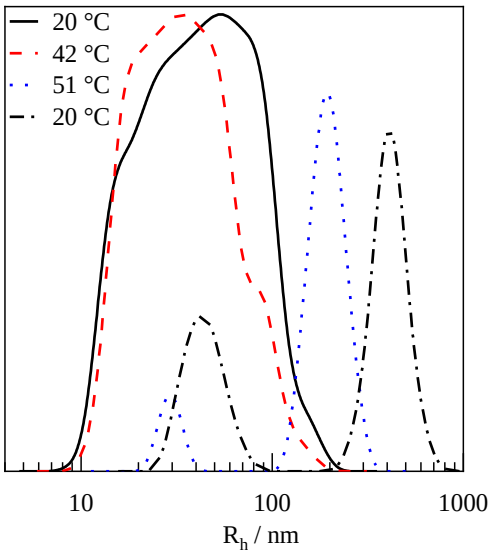

Figure 6 CONTIN plots of 3L3 particles at different temperatures (0.5 g/L, 60 ° detection angle). The solid and dash-dotted black lines represent the samples before and after the heating cycle, respectively.

To determine the morphology of the coagulated particles, freshly prepared 2L2 and 3L3 dispersions were heated to 50 °C and kept at this temperature for 2 hours. They were cooled at a rate of 1 °C/min to room temperature and analyzed by SANS, WAXS and TEM. The SANS data of the 3L3 dispersion (Figure 7A) could not be fitted with a spherical model. Large deviations were observed at low q-values (Figure 7 A inset) and a core-shell cylinder model gave a much better fit. The slope of approximately -2 (log-log) at low-q values is characteristic of elongated objects with a finite cross-section. Using a cylinder model to characterize these particles, the cross-sectional radius obtained is 16 nm, i.e. just a slight reduction compared to the size of the spheres before heating (17.5 nm). A TEM micrograph of 3L3 particles after heat treatment (Figure S 4-1) confirms the presence of large objects of different shapes, including cylindrical objects. In contrast SANS data of a 2L2 dispersion after heat treatment coincide with those of pristine particles (Figure 7 B) confirming that 2L2 particles do not coagulate upon heating,

in accordance with their more compact morphology deduced from SANS data. WAXS analysis of the 3L3 particles before and after treatment indicated that the PiPOx chains did not crystallize upon heat treatment (see Figure S 5-1).

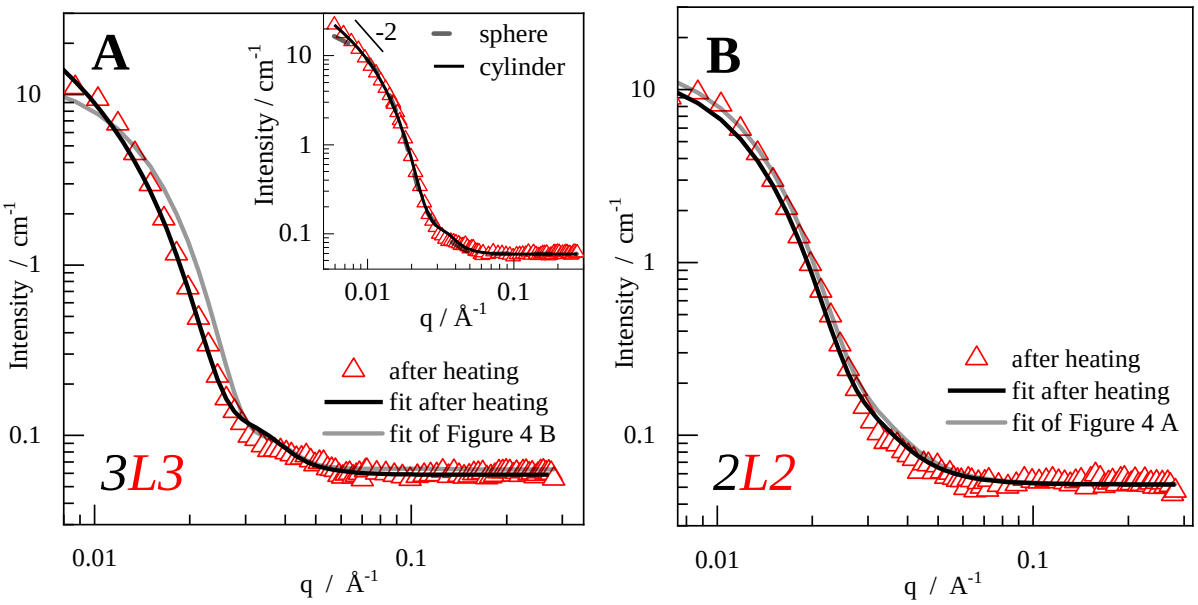

Figure 7 SANS data of the PiPOx-b-PLA dispersions (5 g/L, D_2O) after keeping at 50 °C for 2 hours, measured at 20 °C. The black lines are fits to the models described in the text and the grey lines are the respective fits of Figure 4 (pristine particles) for comparison. The inset in (A) compares directly the fits of a sphere and cylinder model for the SANS data after heating, with an indication of the -2 slope at low *q*-values.

Conclusions:

Compared to most amphiphilic block copolymers, the assembly of PiPOx-*b*-PLA in water presents distinctive characteristics by virtue of the miscibility of the two blocks in the bulk. Importantly, they do not adopt the typical core-shell morphology whereby the hydrophobic and hydrophilic blocks are segregated, respectively, in the core and in the shell of a nanoparticle. The core of PiPOx-*b*-PLA nanoparticles dispersed in water consists of associated PiPOx/PLA chains held together by dipole/dipole

interactions. Their colloidal stability in water results from the presence of hydrated PiPOx loops and tails at the interface between the core and the aqueous medium. The composition and molar mass of the diblock copolymer subtly modify the morphology, bringing about unique properties, highlighted by the remarkable thermal response of the aqueous dispersions: PiPOx-*b*-PLLA dispersions with a short PiPOx block are stable upon heating to 80 °C, a temperature well in excess of the cloud point of PiPOx, with no increase in turbidity; PiPOx-*b*-PDLLA nanoparticles coagulate upon heating and form larger objects of various shapes that do not disintegrate into the pristine nanoparticles upon cooling.

We recall that this unique morphology was adopted by over ten PiPOx-*b*-PLA copolymers of different sizes and compositions following the identical kinetically-controlled experimental protocol: fast addition of a concentrated copolymer solution in tetrahydrofuran into water at room temperature. We currently explore the impact of the preparation method on the nanoparticles morphology and properties. Given the biocompatibility of PLA and the non-toxicity of PiPOx, one may envisage using PiPOx-*b*-PLA nanoparticles as delivery agents. This raises the interesting question of the ability of PiPOx/PLA mixed phases to accommodate, and release, active agents. The complexation-driven assembly of diblock copolymers offers fundamental challenges and practical opportunities that merit further studies.

Conflict of interest:

No conflict of interest to declare.

Supporting information:

This document is supplemented with supporting information including solubility of PLA in H_2O/THF mixtures, particle stability at room temperature, detailed light scattering results, TEM of a 3L3 dispersion after heating and WAXS analysis of freeze-dried 3L3 dispersions.

Acknowledgements:

This work was supported by Tekes/Finland (Project number: 1921/31/2012). The use of the facilities and expertise of the CryoEM unit, member of Biocenter Finland and Instruct-FI, is gratefully acknowledged. FMW acknowledges financial support from the World Premier International Research Center Initiative (WPI), operated by the Ministry of Education, Culture, Sports, Science and Technology (MEXT), Japan, and from the Finnish Distinguished Professor ship grant (TEKES).

References:

(1) Hadjichristidis, N.; Pispas, S.; Floudas, G. *Block Copolymers: Synthetic Strategies, Physical Properties, and Applications*; John Wiley & Sons, Inc., 2003.

(2) Hebbeker, P.; Steinschulte, A. A.; Schneider, S.; Plamper, F. A. Balancing Segregation and Complexation in Amphiphilic Copolymers by Architecture and Confinement. *Langmuir* **2017**, *33* (17), 4091–4106. https://doi.org/10.1021/acs.langmuir.6b04602.

(3) Pooch, F.; Sliepen, M.; Svedstrom, K. J.; Korpi, A.; Winnik, F. M.; Tenhu, H. Inversion of Crystallization Rates in Miscible Block Copolymers of Poly(Lactide)-Block-Poly(2-Isopropyl-2-Oxazoline). *Polym. Chem.* **2018**, *9* (14), 1848–1856. https://doi.org/10.1039/C8PY00198G.

(4) Fedors, R. F. A Method for Estimating Both the Solubility Parameters and Molar Volumes of Liquids. *Polym. Eng. Sci.* **1974**, *14* (2), 147–154. https://doi.org/10.1002/pen.760140211.

(5) Meyer, M.; Antonietti, M.; Schlaad, H. Unexpected Thermal Characteristics of Aqueous Solutions of Poly(2-Isopropyl-2-Oxazoline). *Soft Matter* **2007**, *3* (4), 430–431. https://doi.org/10.1039/B616678D.

(6) Diab, C.; Akiyama, Y.; Kataoka, K.; Winnik, F. M. Microcalorimetric Study of the Temperature-Induced Phase Separation in Aqueous Solutions of Poly(2-Isopropyl-2-Oxazolines). *Macromolecules* **2004**, *37* (7), 2556–2562. https://doi.org/10.1021/ma0358733.

(7) Uyama, H.; Kobayashi, S. A Novel Thermo-Sensitive Polymer. Poly(2-Iso-Propyl-2-Oxazoline). *Chem. Lett.* **1992**, *21* (9), 1643–1646. https://doi.org/10.1246/cl.1992.1643.

(8) Zhou, Y.; Tang, H.; Wu, P. Intra-Molecular Interactions Dominating the Dehydration of a Poly(2-Isopropyl-2-Oxazoline)-Based Densely Grafted Polymer Comb in Aqueous Solution and Hysteretic Liquid-Liquid Phase Separation. *Phys. Chem. Chem. Phys.* **2017**, *19* (9), 6626–6635. https://doi.org/10.1039/C6CP08574A.

(9) Rudolph, T.; Lühe, M. von der; Hartlieb, M.; Norsic, S.; Schubert, U. S.; Boisson, C.; D'Agosto, F.; Schacher, F. H. Toward Anisotropic Hybrid Materials: Directional Crystallization of Amphiphilic Polyoxazoline-Based Triblock Terpolymers. *ACS Nano* **2015**, *9* (10), 10085–10098. https://doi.org/10.1021/acsnano.5b03660.

(10) Rudolph, T.; Nunns, A.; Stumpf, S.; Pietsch, C.; Schacher, F. H. Hierarchical Self-Assembly of Double-Crystalline Poly(Ferrocenyldimethylsilane)-Block-Poly(2-Iso-Propyl-2-Oxazoline) (PFDMS-b-PiPrOx) Block Copolymers. *Macromol. Rapid Commun.* **2015**, *36* (18), 1651–1657. https://doi.org/10.1002/marc.201500245.

(11) Park, J.-S.; Akiyama, Y.; Yamasaki, Y.; Kataoka, K. Preparation and Characterization of Polyion Complex Micelles with a Novel Thermosensitive Poly(2-Isopropyl-2-Oxazoline) Shell via the

Complexation of Oppositely Charged Block Ionomers. *Langmuir* **2007**, *23* (1), 138–146. https://doi.org/10.1021/la061431j.
(12) Korchagina, E. V.; Qiu, X.-P.; Winnik, F. M. Effect of Heating Rate on the Pathway for Vesicle Formation in Salt-Free Aqueous Solutions of Thermosensitive Cationic Diblock Copolymers. *Macromolecules* **2013**, *46* (6), 2341–2351. https://doi.org/10.1021/ma302666e.
(13) An, J.; Liu, X.; Dedinaite, A.; Korchagina, E.; Winnik, F. M.; Claesson, P. M. Effect of Solvent Quality and Chain Density on Normal and Frictional Forces between Electrostatically Anchored Thermoresponsive Diblock Copolymer Layers. *J. Colloid Interface Sci.* **2017**, *487*, 88–96. https://doi.org/10.1016/j.jcis.2016.10.021.
(14) Zschoche, S.; Rueda, J. C.; Binner, M.; Komber, H.; Janke, A.; Appelhans, D.; Voit, B. Temperature- and PH-Dependent Aggregation Behavior of Hydrophilic Dual-Sensitive Poly(2-Oxazoline)s Block Copolymers as Latent Amphiphilic Macromolecules. *Eur. Polym. J.* **2017**, *88*, 623–635. https://doi.org/10.1016/j.eurpolymj.2016.11.014.
(15) Legros, C.; De Pauw-Gillet, M.-C.; Tam, K. C.; Taton, D.; Lecommandoux, S. Crystallisation-Driven Self-Assembly of Poly(2-Isopropyl-2-Oxazoline)-Block-Poly(2-Methyl-2-Oxazoline) above the LCST. *Soft Matter* **2015**, *11* (17), 3354–3359. https://doi.org/10.1039/C5SM00313J.
(16) An, J.; Dėdinaitė, A.; Winnik, F. M.; Qiu, X.-P.; Claesson, P. M. Temperature-Dependent Adsorption and Adsorption Hysteresis of a Thermoresponsive Diblock Copolymer. *Langmuir* **2014**, *30* (15), 4333–4341. https://doi.org/10.1021/la500377w.
(17) Takahashi, R.; Qiu, X.-P.; Xue, N.; Sato, T.; Terao, K.; Winnik, F. M. Self-Association of the Thermosensitive Block Copolymer Poly(2-Isopropyl-2-Oxazoline)-b-Poly(N-Isopropylacrylamide) in Water–Methanol Mixtures. *Macromolecules* **2014**, *47* (19), 6900–6910. https://doi.org/10.1021/ma501538t.
(18) Takahashi, R.; Sato, T.; Terao, K.; Qiu, X.-P.; Winnik, F. M. Self-Association of a Thermosensitive Poly(Alkyl-2-Oxazoline) Block Copolymer in Aqueous Solution. *Macromolecules* **2012**, *45* (15), 6111–6119. https://doi.org/10.1021/ma300969w.
(19) Salzinger, S.; Huber, S.; Jaksch, S.; Busch, P.; Jordan, R.; Papadakis, C. M. Aggregation Behavior of Thermo-Responsive Poly(2-Oxazoline)s at the Cloud Point Investigated by FCS and SANS. *Colloid Polym. Sci.* **2012**, *290* (5), 385–400. https://doi.org/10.1007/s00396-011-2564-z.
(20) Zhou, Y.; Wu, P. Block Length-Dependent Phase Transition of Poly(N-Isopropylacrylamide)-b-Poly(2-Isopropyl-2-Oxazoline) Diblock Copolymer in Water. *Polymer* **2018**, *153*, 250–261. https://doi.org/10.1016/j.polymer.2018.08.027.
(21) Kondo, M.; Takahashi, R.; Qiu, X.-P.; Winnik, F. M.; Terao, K.; Sato, T. Small-Angle X-Ray Scattering from the Concentrated Bulk Phase Separated from an Amphiphilic Block-Copolymer Solution. *Polym. J.* **2017**, *49*, 385.
(22) Saini, P.; Arora, M.; Kumar, M. N. V. R. Poly(Lactic Acid) Blends in Biomedical Applications. *Adv. Drug Deliv. Rev.* **2016**, *107*, 47–59. https://doi.org/10.1016/j.addr.2016.06.014.
(23) Santoro, M.; Shah, S. R.; Walker, J. L.; Mikos, A. G. Poly(Lactic Acid) Nanofibrous Scaffolds for Tissue Engineering. *Adv. Drug Deliv. Rev.* **2016**. https://doi.org/10.1016/j.addr.2016.04.019.
(24) Tyler, B.; Gullotti, D.; Mangraviti, A.; Utsuki, T.; Brem, H. Polylactic Acid (PLA) Controlled Delivery Carriers for Biomedical Applications. *Adv. Drug Deliv. Rev.* **2016**, *107*, 163–175. https://doi.org/10.1016/j.addr.2016.06.018.
(25) Pretula, J.; Slomkowski, S.; Penczek, S. Polylactides—Methods of Synthesis and Characterization. *Adv. Drug Deliv. Rev.* **2016**. https://doi.org/10.1016/j.addr.2016.05.002.

(26) Jain, A.; Kunduru, K. R.; Basu, A.; Mizrahi, B.; Domb, A. J.; Khan, W. Injectable Formulations of Poly(Lactic Acid) and Its Copolymers in Clinical Use. *Adv. Drug Deliv. Rev.* **2016**, *107*, 213–227. https://doi.org/10.1016/j.addr.2016.07.002.
(27) Nicolas, J.; Mura, S.; Brambilla, D.; Mackiewicz, N.; Couvreur, P. Design, Functionalization Strategies and Biomedical Applications of Targeted Biodegradable/Biocompatible Polymer-Based Nanocarriers for Drug Delivery. *Chem. Soc. Rev.* **2013**, *42* (3), 1147–1235. https://doi.org/10.1039/C2CS35265F.
(28) Lee, B. K.; Yun, Y.; Park, K. PLA Micro- and Nano-Particles. *Adv. Drug Deliv. Rev.* **2016**. https://doi.org/10.1016/j.addr.2016.05.020.
(29) Hsiue, G.-H.; Wang, C.-H.; Lo, C.-L.; Wang, C.-H.; Li, J.-P.; Yang, J.-L. Environmental-Sensitive Micelles Based on Poly(2-Ethyl-2-Oxazoline)-b-Poly(l-Lactide) Diblock Copolymer for Application in Drug Delivery. *Int. J. Pharm.* **2006**, *317* (1), 69–75. https://doi.org/10.1016/j.ijpharm.2006.03.002.
(30) Shieh, M.-J.; Peng, C.-L.; Chiang, W.-L.; Wang, C.-H.; Hsu, C.-Y.; Wang, S.-J. J.; Lai, P.-S. Reduced Skin Photosensitivity with Meta-Tetra(Hydroxyphenyl)Chlorin-Loaded Micelles Based on a Poly(2-Ethyl-2-Oxazoline)-b-Poly(d,l-Lactide) Diblock Copolymer in Vivo. *Mol. Pharm.* **2010**, *7* (4), 1244–1253. https://doi.org/10.1021/mp100060v.
(31) Lee, S. C.; Chang, Y.; Yoon, J.-S.; Kim, C.; Kwon, I. C.; Kim, Y.-H.; Jeong, S. Y. Synthesis and Micellar Characterization of Amphiphilic Diblock Copolymers Based on Poly(2-Ethyl-2-Oxazoline) and Aliphatic Polyesters1. *Macromolecules* **1999**, *32* (6), 1847–1852. https://doi.org/10.1021/ma981664k.
(32) Schärtl, W. *Light Scattering from Polymer Solutions and Nanoparticle Dispersions*; Springer Berlin Heidelberg, 2007.
(33) Agrawal, S. K.; Sanabria-DeLong, N.; Tew, G. N.; Bhatia, S. R. Structural Characterization of PLA−PEO−PLA Solutions and Hydrogels: Crystalline vs Amorphous PLA Domains. *Macromolecules* **2008**, *41* (5), 1774–1784. https://doi.org/10.1021/ma070634r.
(34) Heald, C. R.; Stolnik, S.; Kujawinski, K. S.; De Matteis, C.; Garnett, M. C.; Illum, L.; Davis, S. S.; Purkiss, S. C.; Barlow, R. J.; Gellert, P. R. Poly(Lactic Acid)−Poly(Ethylene Oxide) (PLA−PEG) Nanoparticles: NMR Studies of the Central Solidlike PLA Core and the Liquid PEG Corona. *Langmuir* **2002**, *18* (9), 3669–3675. https://doi.org/10.1021/la011393y.
(35) Pagels, R. F.; Edelstein, J.; Tang, C.; Prud'homme, R. K. Controlling and Predicting Nanoparticle Formation by Block Copolymer Directed Rapid Precipitations. *Nano Lett.* **2018**, *18* (2), 1139–1144. https://doi.org/10.1021/acs.nanolett.7b04674.
(36) Shan, J.; Chen, J.; Nuopponen, M.; Tenhu, H. Two Phase Transitions of Poly(N-Isopropylacrylamide) Brushes Bound to Gold Nanoparticles. *Langmuir* **2004**, *20* (11), 4671–4676. https://doi.org/10.1021/la0363938.
(37) Obeid, R.; Tanaka, F.; Winnik, F. M. Heat-Induced Phase Transition and Crystallization of Hydrophobically End-Capped Poly(2-Isopropyl-2-Oxazoline)s in Water. *Macromolecules* **2009**, *42* (15), 5818–5828. https://doi.org/10.1021/ma900838v.
(38) Mössmer, S.; Spatz, J. P.; Möller, M.; Aberle, T.; Schmidt, J.; Burchard, W. Solution Behavior of Poly(Styrene)-Block-Poly(2-Vinylpyridine) Micelles Containing Gold Nanoparticles. *Macromolecules* **2000**, *33* (13), 4791–4798. https://doi.org/10.1021/ma992006i.
(39) Allegra, G.; Ganazzoli, F. Polymer Collapse in Dilute Solution: Equilibrium and Dynamical Aspects. *J. Chem. Phys.* **1985**, *83* (1), 397–412. https://doi.org/10.1063/1.449783.

Table of Content Figure: